

Diagrammatic Monte Carlo method for many-polaron problems

Andrey S. Mishchenko,^{1,2} Naoto Nagaosa,^{1,3} and Nikolay Prokof'ev^{4,2}

¹*Center for Emergent Matter Science, RIKEN (CEMS),
2-12-1 Hirosawa, Wako, Saitama, 351-0198, Japan*

²*Russian Research Center "Kurchatov Institute", 123182 Moscow, Russia*

³*Department of Applied Physics, The University of Tokyo, 7-3-1 Hongo, Bunkyo-ku, Tokyo 113, Japan*

⁴*Department of Physics, University of Massachusetts, Amherst, MA 01003, USA*

(Dated: December 3, 2024)

We introduce the first bold diagrammatic Monte Carlo approach to deal with polaron problems at finite density non-perturbatively, i.e., by including vertex corrections to high orders. Using Holstein model on a square lattice as a prototypical example, we demonstrate that our method is capable of providing accurate results in the thermodynamic limit in all regimes from renormalized Fermi-liquid to single polarons, across the non-adiabatic region where Fermi and Debye energies are of the same order of magnitude. By accounting for vertex corrections the accuracy of theoretical description is increased by orders of magnitude relative to the lowest-order self-consistent Born approximation employed in most studies. We also find that for electron-phonon coupling typical for real materials, the quasiparticle effective mass increases and the quasiparticle residue decreases with increasing the system density.

PACS numbers: 71.38.-k, 31.15.A-, 71.38.Mx

The very nature of a solid state material implies existence of the electron-phonon interaction (EPI). At the formal level, EPI has its origin in Coulomb interaction between the electrons and nuclei and its proper treatment is a notoriously difficult non-perturbative task. In the limit of vanishing electron density we have to deal with the so-called polaron problem: polarons are quasiparticle states with properties significantly (sometimes radically) modified relative to the "bare" particle states by their interaction with the environment. Polarons are found across all fields in physics with the same questions about their dispersion relation, effective mass, quasi-particle residue, etc. being asked for different types of particles, environments and coupling between them [1, 2].

At large electron densities, we face the many-polaron problem, or generic interacting system of electrons and phonons. The standard simplified procedure to deal with EPI in Fermi liquids is based on the adiabatic approximation taking advantage of the small parameter $\gamma = \omega_D/\epsilon_F \sim \sqrt{m_e/m_i} \ll 1$, where ω_D is the Debye frequency, ϵ_F is the Fermi energy, and $m_{e,i}$ are the electronic and ionic masses, respectively. In the adiabatic approximation it is assumed that all interactions between (and with) heavy ions are instantaneously screened by the static dielectric function of a metal, and the phonon spectrum is determined from the corresponding dynamic matrix of a solid. Thus transformed EPI is no-longer singular at small momenta but, nevertheless, remains strong and does not involve natural small parameters in realistic materials; the appropriate dimensionless coupling constant λ (to be defined below) is of the order of unity. [Needless to say that EPI has to be strong enough to be able to mediate *s*-wave superconductivity in a system with Coulomb repulsion.] Such Fermi-liquid parameters as *Z*-factor and effective mass m^* are still

controlled by $\lambda \sim 1$. To leading order, this physics is adequately captured by the self-consistent Born approximation (non-crossing self-energy diagrams) because according to Migdal's theorem [3] vertex corrections are small in the adiabatic parameter γ . Calculating vertex corrections precisely remains a daunting task. Still, it has to be completed in order to (i) establish accuracy limits of the leading approximation, (ii) improve precision of the theoretical description, and (iii) describe cases with $\gamma \sim 1$, intermediate between the Fermi-liquid and single-polaron regimes.

In this work, we will address the many-polaron problem by considering Holstein model [4] on a square lattice

$$H = -t \sum_{\langle i,j \rangle} c_i^\dagger c_j + \omega_0 \sum_i b_i^\dagger b_i + g \sum_i c_i^\dagger c_i (b_i^\dagger + b_i) . \quad (1)$$

We employ standard notations for electron/phonon creation (and annihilation) operators c_i^\dagger/b_i^\dagger . Here t is the nearest neighbor hopping amplitude, ω_0 is the energy of the local optical mode, and g is the strength of EPI. It is convenient to characterize EPI using dimensionless parameter $\lambda = g^2/(4\omega_0 t)$. In what follows the lattice constant a , amplitude t , and Planck's constant \hbar , will be used as units of length, energy, and time, respectively. In the single polaron limit the crossover from weak- to strong-coupling regimes occurs at $\lambda_c \approx 1$. More specifically, the formation of the bipolaron bound state is predicted to occur at $\lambda \approx 0.5$ [5].

It should be noted that a consistent theory of EPI cannot be separated from Coulomb forces between the electrons. Indeed, acoustic phonons in metals do not even exist in the absence of EPI since their energies are shifted all the way up to the ionic plasma frequency. Once electron-phonon and Coulomb interactions between the

electrons are accounted for, the acoustic spectrum is recovered back due to screening of long-range forces [6]. When further progress is made by separating effects of electron-electron and electron-phonon interactions [3, 7], double-counting is dealt with approximately by excluding static electronic polarization terms from the renormalization of phonon propagators. As a result, the effects of EPI on crystal vibrations turn out to be small in the adiabatic parameter γ , but accounting for the remaining terms in the phonon self-energy after that is, strictly speaking, an ill-defined procedure in the absence of electron-electron interactions. Given this subtlety, numerous work simply neglects all effects of EPI on the phonon subsystem, and here we follow the same route (for the most part).

Over the last two decades a significant progress has been made in developing a variety of unbiased numerical methods for single polarons in the context of the EPI Hamiltonian [8–11] (see also Ref. [12, 13] for recent reviews). While these methods provide extremely accurate description of nearly all aspects of polaron physics, in their present form none is suitable for performing precise calculations for finite-density systems all the way from single polarons $\gamma \gg 1$ to the Fermi-liquid with $\gamma \ll 1$. The solution described in this work is based on recent developments in the Bold Diagrammatic Monte Carlo (BDMC) technique [14–16] that takes full advantage of field theoretical methods to compute skeleton (i.e., irreducible and fully renormalized) self-energy diagrams to higher and higher orders using stochastic sampling. By applying BDMC to solve Holstein model at finite chemical potential and temperature on a square lattice, we observe that expansion in skeleton diagrams for self-energy is convergent not only in the single-polaron and Fermi-liquid limits (as expected) but also in the non-adiabatic parameter regime when $\gamma \sim 1$. By accounting for vertex corrections, the accuracy of theoretical description is radically improved from about 5% (for the standard lowest-order treatment) down to 0.2%. Contrary to expectations that quasiparticle properties are most strongly renormalized in the single polaron limit, we find that the opposite is true—the effective mass increases and the quasiparticle residue decreases with increasing the electron density. Our results should be considered as a first successful attempt to deal with EPI at finite electron densities in a non-perturbative way, and an important step towards fully self-consistent treatment of both electron-phonon and electron-electron interactions required for material science.

Our implementation of BDMC is based on standard irreducible self-energy diagrams in terms of exact propagators G and D for the electronic and vibrational degrees of freedom, respectively, the so-called G^2W expansion [17], in close similarity with the formulation used for quantum spin models [16]. In the present case, screened inter-particle interactions are replaced with D and, thus,

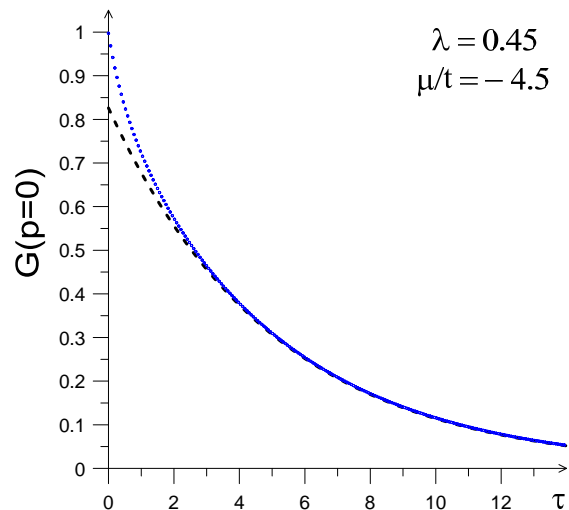


FIG. 1: Color online: Green function of a single polaron with zero momentum at $\lambda = 0.45$, $\mu/t = -4.5$ and zero temperature obtained by the BDMC technique (blue dots). It is compared to the asymptotic behavior $G_{\tau \rightarrow \infty}(p=0) = Z_s \exp[-E_s \tau]$ (dashed line) with $Z_s = 0.826$ and $E_s = -0.302$ calculated by the conventional single-polaron diagrammatic MC approach [9]. All error bars are smaller than symbol sizes.

it is more appropriate to denote this expansion as G^2D instead of G^2W , or G^2D_0 , if the renormalization of D is ignored (see discussion above). Since all obvious differences in the microscopic Hamiltonian are accounted for at the level of “bare” electron and phonon propagators in Dyson equations, the G^2D and G^2W expansions appear identical and we will not reproduce it here.

The essence of the BDMC method and algorithm (described in full detail in Ref. [16]) is to sample the configuration space of skeleton Feynman diagrams for electronic, Σ , and vibrational, Π , self-energies to higher- and higher-order using Monte Carlo (MC) techniques, with feedback loops in terms of Dyson equations. In the best case scenario, physical answers converge as the diagram order is increased. Even though the number of diagrams of order N increases factorially, they may all cancel each other to ensure that the BDMC technique produces converged (or subject to re-summation methods) results. Establishing convergence properties of the skeleton expansion for the EPI system is the most important methodological result of this work. We refer studies of the superfluid instability to future work and thus limit ourselves here to the coupling constant $\lambda = 0.45$, just below the threshold for the bipolaron formation. Given that the bandwidth of the tight-binding model is $W = 8t$, we fix $\omega_0 = 0.5t$, low enough to guarantee that we can reproduce the Fermi-liquid regime with $\gamma \ll 1$.

Feynman diagrams are typically formulated in the thermodynamic limit. In practice, for reasons of convenient data handling, in this work we choose to consider

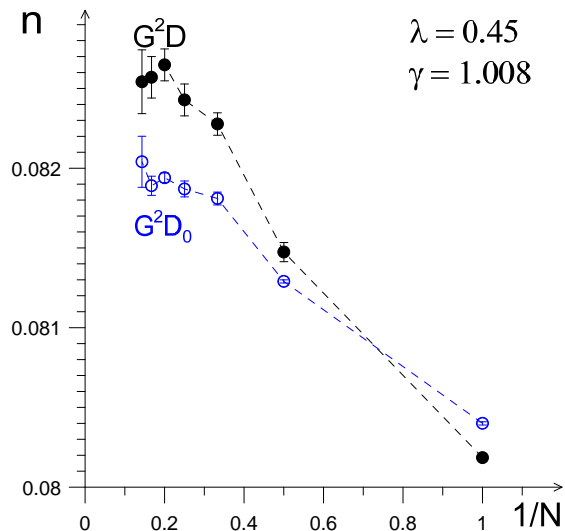


FIG. 2: Electron density calculated from diagrams up to order N without (open blue squares) and with (filled black circles) self-consistent renormalization of phonons at $\lambda = 0.45$, $\gamma = 1.008$, and $T = 0.01$. We subtracted the static local polarization operator of the ideal electron gas at the same density from the phonon self-energy in order to mimic the standard material science protocol [6] where this contribution is already accounted for in the original phonon spectrum of Holstein model.

finite system sizes $L^2 = 128^2$ with periodic boundary conditions, large enough to ensure that final answers do not depend on L within error bars.

We start with establishing convergence properties of the BDMC scheme. In the single-polaron limit the diagrammatic expansion is sign-positive and convergence is guaranteed. The difference between the more conventional diagrammatic approach [8, 9] and BDMC is that all momenta are simulated in a single run and the number of diagrams at any given order is reduced in the latter. In this regime, one is not limited by the maximum diagram order and all error bars are statistical in nature. In Fig. 1 we show that the BDMC approach perfectly reproduces known results for polarons.

According to Migdal's theorem, we also expect nice convergence properties in the Fermi-liquid regime (at least up to diagram orders comparable to $1/\gamma \gg 1$). It is thus crucial to study what happens in the non-adiabatic regime $\gamma \sim 1$. In Fig. 2 we present our data for particle density at fixed chemical potential $\mu/t = -3.75$ as a function of the maximum diagram order accounted for in the simulation; this chemical potential corresponds to $\gamma \approx 1.008$, with ϵ_F determined from the renormalized spectrum at the end of the calculation. From this plot we conclude that the skeleton series are convergent since most changes are exhausted by going from first- to fourth-order diagrams; all 2,017,881 eighth-order diagrams [17] cancel each other within the error bars. It is

worth emphasizing here, that the lowest-order result all by itself is meaningless despite the fact that it is capturing most of the answer because its limits of accuracy can be established only through higher-order calculations. In addition, Fig. 2 makes it clear that the accuracy of the theoretical description is improved at least by an order of magnitude (down to a fraction of a percent) if vertex corrections up to forth-order are accounted for. Further improvements can be achieved only at the expense of increased simulation time due to factorial growth of computational complexity with the diagram order. The rest of the data presented in this work were obtained by performing simulations up to fourth-order (with additional checks at selected points that six-order results are the same within the error bars).

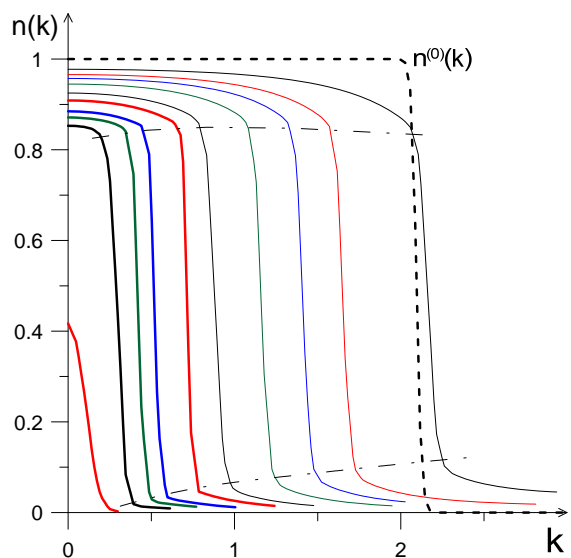


FIG. 3: Color online: Momentum distributions for various electron densities per site n (from right to left: $n=0.6498$, 0.4055 , 0.3026 , 0.2086 , 0.1222 , 0.08169 , 0.04323 , 0.02846 , 0.01413 , 0.001416) at $\lambda = 0.45$. For $n > 0.1$ we consider $T/t = 0.025$ (thin lines); for $n < 0.1$ the temperature is reduced down to $T/t = 0.01$ (thick lines). The dashed line corresponds to the ideal gas case at $T/t = 0.025$ and $\mu/t = -1$. With dash-dotted lines we show (approximately) the locations of the $T = 0$ jumps in the distribution function.

In Fig. 3 we present the entire evolution of the electron momentum distribution $n(k)$ from high ($\gamma < 1/6$) to low ($\gamma \approx 6$) densities with the characteristic jump at the Fermi momentum (smeared by finite-temperature effects). At the lowest density the conventional Fermi-distribution transforms into the Gaussian distribution characteristic of the dilute polaron gas at finite temperature $T = 0.01t > \epsilon_F$. By looking at Fig. 3, one might think that the quasiparticle residue Z decreases from high to low densities, judging by the value of $1 - n(k=0)$ and by invoking an argument that Pauli-principle restric-

tions at the Fermi surface reduce the amount of spectral weight transfer to incoherent continuum and quasiparticle “dressing”. This intuition turns out to be completely wrong because one has to look at the discontinuity of the distribution function at the Fermi surface in the limit of $T \rightarrow 0$ (see dashed-dotted lines in Fig. 3).

To deduce the quasiparticle residue and effective mass at the Fermi surface we perform standard data processing for the proper self-energy defined on Matsubara frequencies $\omega_m = 2\pi T(m + 1/2)$ at the Fermi surface. First, we extrapolate the real part of $\Sigma(\mathbf{k}, m)$ to the $m = -1/2$ limit using parabolic fits with respect to m to obtain $\Sigma'(\mathbf{k})$. We then solve numerically the equation $\epsilon(\mathbf{k}) - \mu + \Sigma'(\mathbf{k}) = 0$, where $\epsilon(\mathbf{k}) = -2[\cos(k_x) + \cos(k_y)]$ is the bare tight-binding dispersion relation, to determine the shape of the Fermi surface (FS) in the interacting system. Similarly, for any point on the FS, we obtain the quasiparticle residue by extrapolating data for $b(\mathbf{k}, m) = -\Sigma''(\mathbf{k}, m)/\omega_m$ to the $m = -1/2$ limit; according to the Fermi-liquid theory, $Z(\mathbf{k}) = [1 + b(\mathbf{k})]^{-1}$ where $b = -\lim_{\omega \rightarrow 0} \partial \Sigma(\mathbf{k}, \omega) / \partial \omega$. Next, the FS velocity is obtained by taking the gradient along the normal direction to FS: $v_F(\mathbf{k}_F) = Z(\mathbf{k}_F) \nabla_{\perp} [\epsilon(\mathbf{k}) - \mu + \Sigma'(\mathbf{k})]_{k \in FS}$. Finally, the effective mass renormalization, m_0/m^* , is deduced by dividing $v_F(\mathbf{k}_F)$ by the corresponding FS velocity of the non-interacting gas at the same density. Except for the largest density, we find that the anisotropy in Z and m^*/m_0 is very small.

Our results for Z and m^*/m_0 are shown in Fig. 4. Contrary to naive expectations (for single polarons vertex corrections are the strongest and lead to increased renormalization of quasiparticle properties), the data unambiguously indicate that quasiparticles are more heavily “dressed” in the Fermi-liquid regime. [Further proof that our Fermi-liquid type analysis is correct and simulation temperatures are low enough for this analysis to be valid is provided by excellent agreement with the single-polaron ($T = 0$) results in the low-density limit.] We interpret these results as follows: scattering restrictions imposed by the Pauli principle do not overcome the increased low-energy phase space available for scattering at finite, as opposed to zero, particle momenta on the FS, not to mention that higher-order terms also admit dressing by particle-hole pairs. The effective mass renormalization mostly follows Z because Zm^*/m_0 is essentially constant and very close to unity over the entire density range, reflecting locality (weak momentum dependence) of the self-energy in Holstein model.

To conclude, we established that the bold diagrammatic Monte Carlo technique provides an effective method for solving the many-polaron (or generic interacting electron-phonon) problem with high and controlled accuracy. The skeleton series converge for moderate values of the dimensionless coupling λ even in the non-adiabatic parameter regime, and final results for Fermi-liquid parameters can be obtained with sub percent ac-

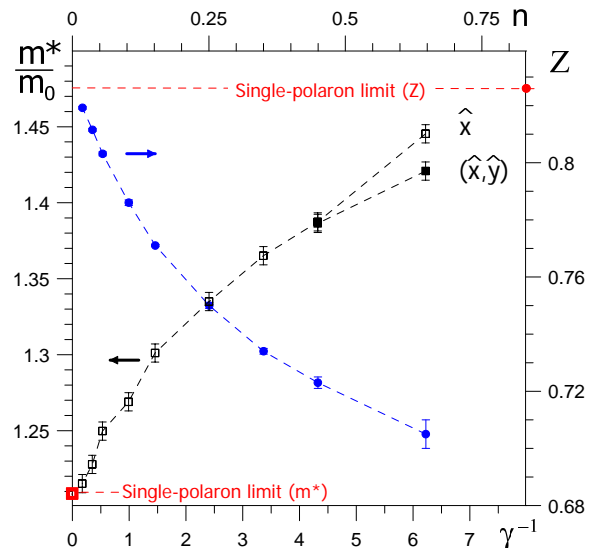


FIG. 4: Color online: Effective mass along \hat{x} (black open squares) and (\hat{x}, \hat{y}) (black filled squares) directions and quasiparticle residue (blue circles) as functions of the adiabatic parameter at $\lambda = 0.45$ deduced from the same set of simulations as in Fig. 3. The upper horizontal axis provides an approximate density scale. Error bars for Z at large γ^{-1} are not statistical; they indicate the anisotropic spread of Z values on the FS. The anisotropy of the effective mass is significant only for the largest density, while for all other points the anisotropy is unmeasurably small.

curacy after vertex corrections are accounted for. We find that the quasiparticle “dressing” is enhanced in the Fermi-liquid regime relative to the single-polaron case. Future work should aim at adding electron-electron interactions into the picture, studies of the phonon spectrum renormalization, superconducting instability, etc.

We thank B. Svistunov for discussions. This work was supported by the Simons Collaboration on the Many Electron Problem, the National Science Foundation under the grant PHY-1314735, and the MURI Program “New Quantum Phases of Matter” from AFOSR. N.N. is supported from the Japan Society for the Promotion of Science (JSPS) through the ‘Funding Program for World-Leading Innovative R&D on Science and Technology (FIRST Program), and Grant-in-Aids for Scientific Research (No.24224009) from the Ministry of Education, Culture, Sports, Science and Technology (MEXT).

-
- [1] L.D. Landau, Phys. Z. Sowjetunion **3**, 664 (1933).
 - [2] J. Appel, in *Solid State Physics*, eds. H. Ehrenreich, F. Seitz, and D. Turnbull, Academic, New York, Vol. **21**, (1968).
 - [3] A.B. Migdal, JETP **34**, 1438 [Sov. Phys. JETP **7**, 996] (1958).
 - [4] T. Holstein, Ann. Phys. (N.Y.) **8**, 325 (1959).

- [5] A. Macridin, G. A. Sawatzky, and M. Jarrel, Phys. Rev. **B 69**, 245111 (2004).
- [6] E.G. Brovman and Yu. Kagan, JETP **52**, 557 [Sov. Phys. JETP **25**, 365] (1967).
- [7] G.M. Eliashberg, JETP **38**, 966 [Sov. Phys. JETP **11**, 696] (1960).
- [8] N.V. Prokof'ev and B.V. Svistunov, Phys. Rev. Lett. **81**, 2514 (1998).
- [9] A.S. Mishchenko, N.V. Prokof'ev, A. Sakamoto, and B.V. Svistunov, Phys. Rev. B **62**, 6317 (2000).
- [10] P.E. Kornilovitch, Phys. Rev. Lett. **81**, 5382 (1998).
- [11] J. Bonca, S. A. Trugman, and I. Batistic, Phys. Rev. B **60**, 1633 (1999).
- [12] *Polarons in Complex Matter*, edited by A. S. Alexandrov, Springer Series in Material Science (Springer, Dordrecht, 2007)
- [13] *Computational Many-Particle Physics*, edited by H. Fehske, R. Scheider and A. Weisse, Lecture Notes in Physics Vol. 739 (Springer, Berlin Heidelberg, 2008).
- [14] N. Prokof'ev and B.V. Svistunov, Phys. Rev. Lett. **99**, 250201 (2007).
- [15] K. Van Houcke, F. Werner, E. Kozik, N. Prokofev, B. Svistunov, M. Ku, A. Sommer, L. W. Cheuk, A. Schirrotzek, and M. W. Zwierlein, Nature Phys. **8**, 366 (2012).
- [16] S. Kulagin, N. Prokof'ev, O.A. Starykh, B.V. Svistunov, and C.N. Varney, Phys. Rev. Lett. **110**, 070601 (2013); *ibid* Phys. Rev. **B 87**, 024407 (2013).
- [17] L.G. Molinari and N. Manini, Eur. Phys. J. B **51**, 331 (2006).